Journal of Materials Chemistry C

Accepted Manuscript

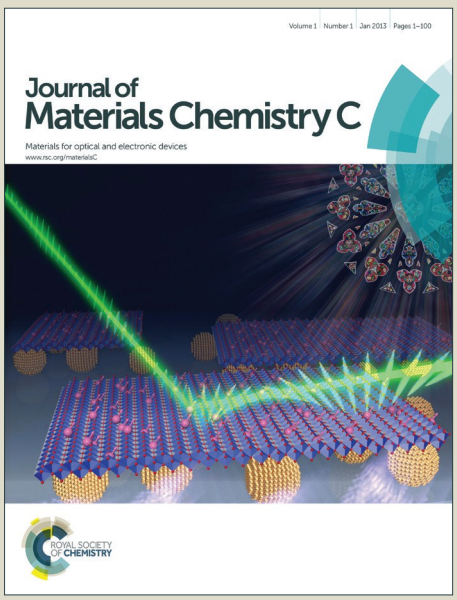

ROYAL SOCIETY OF CHEMISTRY

www.rsc.org/materialsC

Journal Name

Article

Crystallization induced enhanced emission in conformational polymorphs of a rotationally flexible molecule

Received 00th January 20xx,
Accepted 00th January 20xx

DOI: 10.1039/x0xx00000x

www.rsc.org/

Ajith R. Mallia,‡ Ramarani Sethy,‡ Vinayak Bhat and Mahesh Hariharan*

Crystallization of a weakly fluorescent 4-amino-2,2'-bipyridine (AMBPY) in solution phase under ambient conditions afforded three fluorescent conformational polymorphs. Marginal increase in barrier to rotation observed in AMBPY as compared to unsubstituted 2,2'-bipyridine could be attributed to the "buttressing effect" offered by the amino substituent at the meta position. Smaller yet significant difference in energy (0.1-2.6 kJ/mol) with respect to global minima facilitates isolation of AMBPY-I-III polymorphs. Unique nitrogen-nitrogen interaction is observed in two of the polymorphs namely, AMBPY-I and AMBPY-III promoted by cooperative C•••H and N•••H interactions. Crystallization induced enhancement (ca. 5-10 fold) in fluorescence quantum yield of AMBPY polymorphs is observed relative to the solution/amorphous state. Controlling the luminescence properties of molecular solids by tuning their packing arrangements via various interactions is an integral aspect in the construction of novel photo-functional materials.

Tuning and switching the luminescence properties of organic crystalline materials (OCMs) by modulating molecular packing through non-covalent routes is a burgeoning topic of interest.[1] OCMs can find potential applications in the area of organic light emitting diodes, organic field effect transistors, sensors, solid state lasers and biological imaging.[2] Molecular ordering in OCMs play pivotal role in deriving new strategies which could be translated in modulating solid state luminescent properties[3] from collections of molecules. Attempts in modifying material properties via non-covalent[4] inter/intramolecular interactions such as hydrogen bonding, π–π and C-H•••π interactions resulted in conformational/packing polymorphism,[5] structural changes by preserving molecular integrity (phase transition),[3a] disturbing long-range molecular ordering (amorphization)[6] and moderating fluorophore aggregation.[7] Polymorphism is a solid state phenomenon, in which a chemical compound exists in more than one crystalline form without altering its chemical composition.[8] Emission enhancement observed in the aggregated state relative to the monomeric state established by Tang et al. is described as aggregation induced enhanced emission (AIEE).[7, 9] For solids in the crystalline state, emission can be enhanced by means of crystallization and is termed as crystallization induced enhanced emission (CIEE).[10] Our ongoing research in the area of CIEE[11] of near-orthogonal chromophoric dyads[12] possessing significant rotational barrier encouraged us to investigate the solid-state luminescent properties of rotationally flexible 4-amino-2,2'-bipyridine (**AMBPY**). Herein we present conformational polymorphism exhibited by rotationally flexible **AMBPY** derivatives possessing CIEE relative to the solution/amorphous state.

4-amino-2,2'-bipyridine (**AMBPY**) was synthesised as per the reported procedure (Scheme S1, ESI†).[13] Crystallization of **AMBPY** in CH_2Cl_2:hexane (3:1), benzene, and CH_3OH:hexane (2:1) offered three fluorescent conformational polymorphs having needle (**AMBPY-I**), plate (**AMBPY-II**) and rhombus (**AMBPY-III**) features. Single crystal X-ray diffraction analyses of the polymorphs resulted in solvent free crystal systems (See notes and references). Origin of conformational polymorphism in **AMBPY** could be corroborated to the differences in the torsion angle $\Theta_{N2\text{-}C5\text{-}C6\text{-}N1}$ (Fig. 1a) that varies from 179.5°-220.8° with torsional energy barrier of 0.1-2.6 kJ/mol with respect to the global minima (Fig. S1 & Table S1, ESI†).

AMBPY-I crystallizes in an enantiomorphic space group $P6_5$ (hexagonal crystal system) with six molecules in the asymmetric unit (Fig. 1d). N3–H3" (Fig. 1a) of amino group in **AMBPY-I** serve as bifurcated H-bond donors to dictate the packing in three dimension (Fig. 2a). Intermolecular short contacts (lesser than the sum of the Van der Waal radii of constituent atoms)[14] between N2•••H3''–N3 (2.15 Å) and C1•••H3''–N3 (2.72 Å) units bring the nitrogen atoms (N2 and N3) at an interactive distance of 3.01 Å. Unprecedented occurrence of (Fig. 2a & Table S2, ESI†) two nitrogen atoms, sp^2 hy-

School of Chemistry, Indian Institute of Science Education and Research Thiruvananthapuram, CET Campus, Sreekaryam, Thiruvananthapuram, Kerala, India 695016. E-mail: mahesh@iisertvm.ac.in

‡ *These authors contributed equally to the manuscript.*

† Electronic supplementary information (ESI) available:
Synthesis and characterisation of AMBPY, photophysical properties of AMPBPY in solution, amorphous and crystalline state. See DOI: 10.1039/x0xx00000x

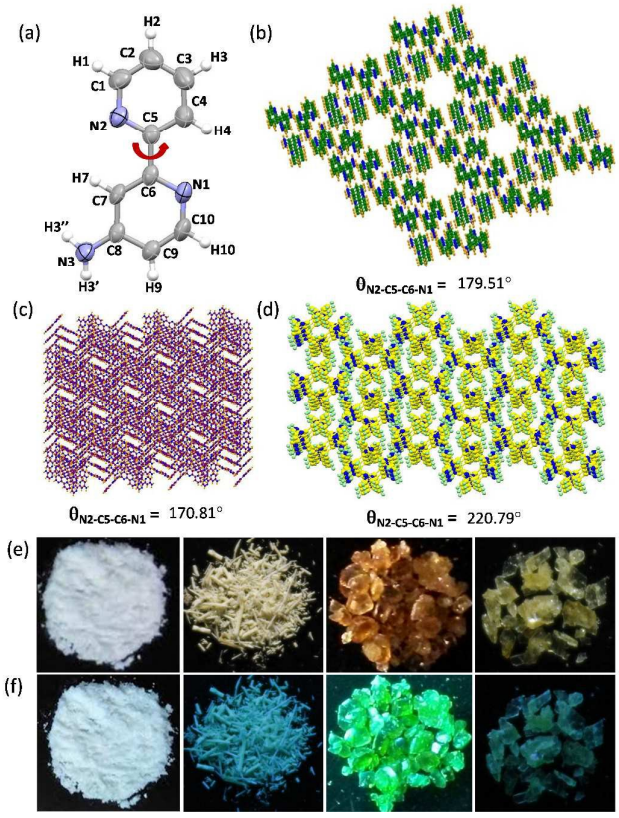

Figure 1. (a) Molecular structure of 4-amino-2, 2′-bipyridine (**AMBPY**); (b-d) three dimensional packing in conformational polymorphs of **AMBPY**; photographs of amorphous **AMBPY** and crystalline **AMBPY-I-III** (e) in the day light and (f) under UV illumination at 365 nm respectively.

bridised nitrogen (N2) and sp^3 hybridised nitrogen (N3), at a distance less than the sum (<3.1 Å) of van der Waals radius could be a consequence of primary short contacts between N2•••H3''–N3 and C1•••H3''–N3. Apart from this, C–H•••π interaction operating at 2.65-2.86 Å further contributes to packing in **AMBPY-I**. **AMBPY-II** crystallizes in tetragonal crystal system with $I4_1$ enantiomorphic space group possessing sixteen molecules in the asymmetric unit. Short contacts (Fig. 2b & Table S2, ESI†) between N1•••H3''–N3 (2.50 Å), N2•••H3'–N3 (2.23 Å), C10•••H3'–N3 (2.84 Å), C5•••H3''–N3 (2.75 Å), and C–H•••π interaction (2.88 Å) direct the three dimensional arrangement in **AMBPY-II**. **AMBPY-III** crystallizes in centrosymmetric space group (*Pccn*) with orthorhombic crystal system having eight molecules in the asymmetric unit. N3–H3' and N3–H3'' units of amino group act as H-bond donors and participate in trifurcated and bifurcated interactions (Fig. 2c & Table S2, ESI†) respectively. Short contacts between N2•••H3'–N3 (1.97 Å), C10•••H3'–N3 (2.55 Å), N2•••H3''–N3 (2.42 Å), C6•••H3''–N3 (2.56 Å) units and dihydrogen interaction H10•••H3'–N3 at a distance of 2.38 Å direct the three dimensional arrangement in **AMBPY-III**. As observed in **AMBPY-I**, the cooperative interactions between N2•••H3'–N3, C10•••H3'–N3 and H10•••H3'–N3 result in bringing N2

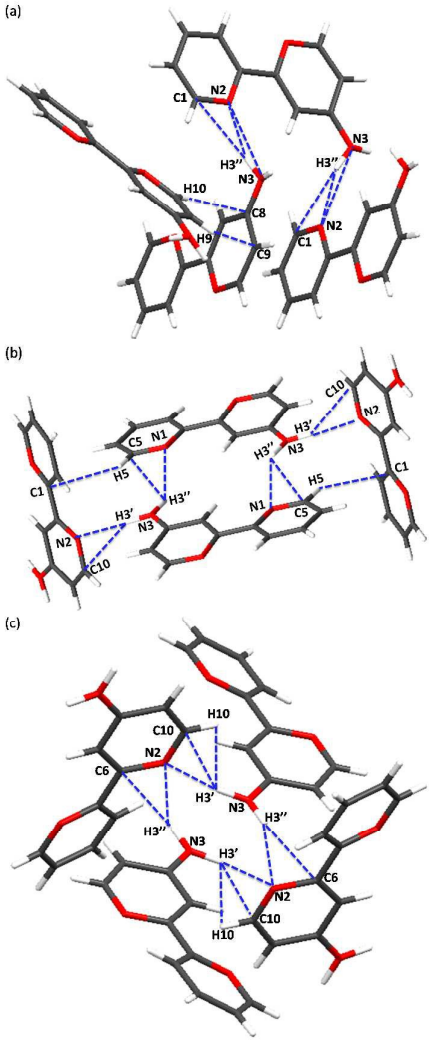

Figure 2. Intermolecular interactions present in (a) **AMBPY-I**, (b) **AMBPY-II** and (c) **AMBPY-III** polymorphs.

and N3 atoms at a distance of 2.92 Å in **AMBPY-III**. Observed diverse packing modes in **AMBPY-I-III** polymorphs, when crystallised from distinct solvents, could be attributed to the dissimilar hydrogen bond donor abilities of the respective solvents (see ESI†).[15] A comparative account of different short range interactions present in the three polymorphs suggest that **AMBPY-II** and **AMBPY-III** are densely packed in comparison with **AMBPY-I** (Fig. 1d). This prompted us to investigate the distribution of void space (pores) present in the polymorphs using Mercury 3.1 software.[16] We observed that needle shaped **AMBPY-I**, possesses pores with cavity size of 8.50-10.02 Å occupying 15.92% of the unit cell with the void volume of 232.18 $Å^3$ (Fig. S2, ESI†), while **AMBPY-II** and **AMBPY-III** are non-porous. Consequently, **AMBPY-I** exhibits a low packing efficiency (PE) of 0.61 whereas **AMBPY-II** and **AMBPY-III** exhibit PE of 0.69 and 0.67 respectively. Sizeable lattice voids such as those observed in **AMBPY-I** is less explored in pure organic solid-state frameworks.[17] Despite substantial lattice voids, which could arise due to desolvation at ambient conditions, resulting in **AMBPY-I** assemblies that are stabilised due to the presence of N•••H–N, C•••H–N and C–H•••π interactions, consistent with earlier

reports.[18] Upon performing X-ray diffraction measurements at 120 K, **AMBPY-I** exhibits residual electron density corresponding to solvent molecules in the voids, however, any attempt to obtain a complete and meaningful model of all the disordered solvent molecules turned out to be unsuccessful.

Hirshfeld surface (HS)[19] and two dimensional fingerprint analyses[20] were employed to investigate the packing motifs existing in the crystal structures of **AMBPY** polymorphs.[21] Distinct two dimensional fingerprint plots obtained for **AMBPY** polymorphs confirm that their packing modes are dissimilar (Fig. 3a-c & Table S3, ESI†). Investigation of 2D-fingerprint plots (Fig. 3d-f) derived from HS analyses demonstrate that C•••N (2.3-3.3%), C•••C (6.4-9.2%), N•••H (15.8-17.5%), C•••H (15.6-23.6 %) and H•••H (44.1-53.1%) interactions dictate the packing in **AMBPY** polymorphs (Fig. S3-S5, ESI†). The sharp spikes and a pair of wings observed in 2D-fingerprint plots of **AMBPY-I-III** polymorphs correspond to N•••H (Fig. S5c,g,k, ESI†) and C•••H interactions (Fig. S5b,f,j, ESI†) respectively. Crystal packing[22] in **AMBPY-I** and **AMBPY-III** comprises of offset, face-to-face infinite π—π interaction and a form of herringbone (edge-to-face, 1.2<ρ<2.7, γ-motif) arrangement (Fig. 3a-c, S6,S8 & Table S4, ESI†). In contrast, **AMBPY-II** exhibits offset and edge-to-face π—π interaction that forms sandwich herringbone arrangement (3.2 <ρ< 4.0). In **AMBPY-I** (ρ = 2.07) offset stacking propagates along '*b*' axis, face-to-face stacking repeat along '*c*' axis, while edge-to-face stacking is along '*a*' axis (Fig. S6a-c, ESI†). Similar to **AMBPY-I**, offset stacking in **AMBPY-III** (ρ = 1.92) is generated along '*a*' axis, face-to-face infinite stacking spreads through '*c*' axis whereas edge-to-face stacking is observed along '*b*' axis (Fig. S8a-c, ESI†). Close packing in **AMBPY-II** (ρ = 3.68) is characteristic of sandwich herringbone arrangement, possessing offset π—π interaction along '*b*' axis and edge-to-face interactions in '*c*' axis (Fig. S7a-c, ESI†). Besides, in **AMBPY-II** molecules close pack in pairs, a common feature that is observed in sandwich herringbone arrangement. The distinct HS (d_{norm}) highlights short intermolecular interactions present in a molecule in terms of diagnostic intense red and orange hot-spots.[23] d_{norm} designates H-bond donors and acceptors, wherein appearance of an intense red spot indicates presence of H-bond acceptor and a faint orange spotdescribes H-bond donor. d_{norm} was generated along '*c*' axis for **AMBPY-I-III** (Fig. S3B, ESI†). Inspection of d_{norm} reveals that the interactions illustrated in the crystal structure analyses could be correlated to the interactions observed from HS analyses. H3' of N3-H3' moiety and H3'' of N3-H3'' unit in **AMBPY-I** and **AMBPY-II** respectively acts as H-bond donors ($d_{H\bullet\bullet\bullet N}$ = 2.05-2.28 Å), while N1 and N2 act as H-bond acceptors ($d_{N\bullet\bullet\bullet H}$ = 1.80-2.20 Å, Fig.S3Ba,b ESI†). In **AMBPY-III**, N1 acts as H-bond acceptor ($d_{H\bullet\bullet\bullet N}$ = 2.19 Å) and H3' of N3-H3' and H3'' of N3-H3'' belonging to two different neighbouring units act as H-bond donor ($d_{N\bullet\bullet\bullet H}$ = 1.22 Å, Fig. S3Bc, ESI†) resulting in a bifurcated hydrogen bonded interactions.

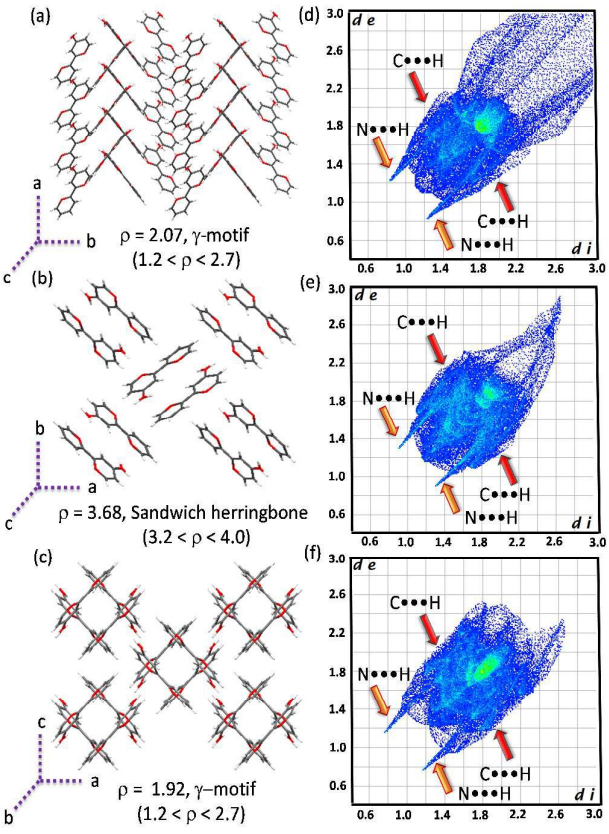

Figure 3. (a), (b), (c) represent close packing in **AMBPY-I-III** polymorphs indicating the values of ρ [(%C•••H)/(%C•••C)],[21] and (d), (e), (f) the corresponding two dimensional fingerprint plots determined from Hirshfeld surface analyses.

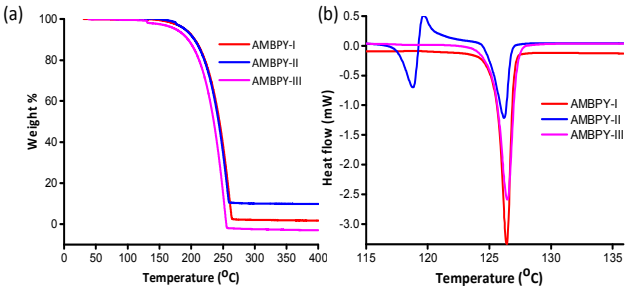

Figure 4. (a) Thermogravimetric and (b) differential scanning calorimetric analyses of **AMBPY** polymorphs.

Powder x-ray diffraction (PXRD) measurements were performed to investigate bulk properties of **AMBPY** polymorphs. Good agreement between experimental and calculated (using Mercury 3.1 software[16]) PXRD patterns for **AMBPY** polymorphs indicates structural homogeneity exhibited by the polymorphs (Fig. S9, ESI†). Thermogravimetric and differential scanning calorimetric analyses were performed to investigate the thermal stability and phase transitions in the polymorphs. **AMBPY-I-III** polymorphs are thermally stable upto 210 °C (Fig. 4a & Table S5, ESI†). The DSC thermograms (Fig. 4b) of **AMBPY-I** and **AMBPY-III** exhibit sharp endothermic peaks at 124.6 and 125.6 °C corresponding to the mel ting transition with enthalpy changes ΔH = 18.9 and 19.1 kJ/mol res pectively. The DSC thermogram of **AMBPY-II** has two endothermic melting transitions; (i) at 118.8 °C with ΔH = 17.4 kJ/mol and (ii) at 126.6 °C having ΔH = 19.8 kJ/mol respectively. Apart from endothermic transitions, an exothermic transition corresponding to the crystallization at 120.2 °C possessing ΔH = -1.8 kJ/mol is also observed for **AMBPY-II**. Observed exothermic transition at 120.2 °C could be attributed to the transformation of metastable **AMBPY-II**

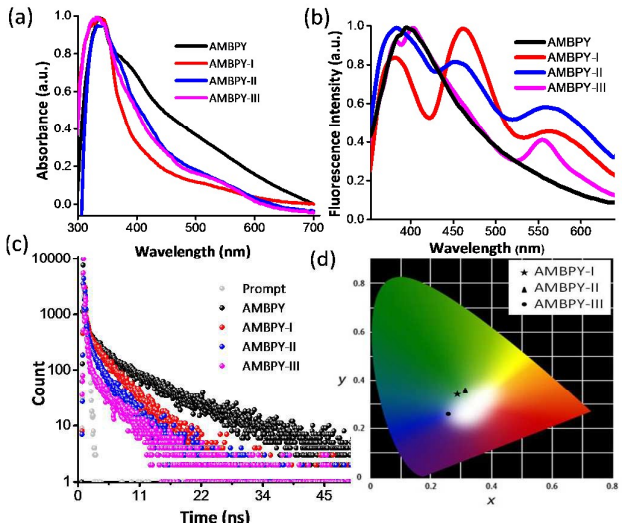

Figure 5. (a) UV-Vis absorption, (b) emission spectra (excited at 330 nm), (c) fluorescence decay profile excited at 375 nm and (d) CIE coordinates for **AMBPY** polymorphs.

to thermodynamically stable **AMBPY-I/III** through enantiotropic transition as reported earlier.[11c, 24]

Solid state photophysical measurements of **AMBPY** polymorphs were performed to investigate distinct luminescence properties. The steady state UV-Vis absorption spectra (Fig. 5a & Table 1) of crystalline **AMBPY-I**, **AMBPY-II**, **AMBPY-III** and amorphous **AMBPY** have absorption bands centred at 338, 341, 330 and 336 nm respectively which could be attributed to the π-π* transition[3a, 25] as confirmed from theoretical calculations employing B3LYP-D3/6-31G**+ level of theory (Fig. S10, ESI†). Appearance of absorption bands of **AMBPY** polymorphs in the same region suggests presence of similar photoexcitation processes in the polymorphs. Upon excitation at 330 nm, amorphous **AMBPY** shows emission (Fig. 5b & Table 1) centred at 400 nm while **AMBPY** polymorphs exhibit vibronically resolved emission in comparison to the solution state(Fig. S11, ESI†). The dissimilar photophysical properties in the solution state could be dictated by the differences in (i) π-π (face-exhibited by **AMBPY-I-III** polymorphs in the solid state in comparison to the to-face) interactions and/or (ii) intramolecular torsional angle, $\Theta_{N2\text{-}C5\text{-}C6\text{-}N1}$. Emission spectrum of **AMBPY-I** and **II**, when excited at 330 nm, consist of three peaks centred at 380, 462 and 565 nm, while **AMBPY-III** possesses peaks centred at 372 and 555 nm (Fig. S5-S6, Table S3, ESI†). Time correlated single photon counting measurements were performed to investigate the fluorescence lifetimes, by exciting the samples at 375 nm (Fig. 5c & Table 1). The lifetime decay profiles follow a bi-exponential fit with an average lifetime of 4.69, 3.48, 1.89 and 1.79 ns respectively for **AMBPY**, **AMBPY-I**, **AMBPY-II** and **AMBPY-III**. The biexponential nature of fluorescence lifetimes could be attributed to the presence of two different predominant packing arrangements within the same polymorph. The CIE[26] coordinates estimated for **AMBPY-I**, **AMBPY-II** and **AMBPY-III** are (0.30, 0.35), (0.31, 0.34) and (0.27, 0.26) respectively (Fig. 5d). This is clearly suggestive of the fact that the conformational polymorphs **AMBPY-I** and **AMBPY-II** are near-white light emitting (0.33, 0.33).

Fluorescence quantum yield (Φ_f) measurements of **AMBPY** polymorphs in the solid state afforded Φ_f as tabulated in Table 1. It

Table 1. Comparison of photophysical properties of **AMBPY**.

Samples	Shape	λ_{abs}, nm	λ_{ems}, nm	τ[a], ns	Φ_f (± 0.02 %)
AMBPY	Amorphous	336	400	4.697	0.6
AMBPY-I	Needle	338	379, 462, 564	3.486	2.4
AMBPY-II	Plate	341	386, 455, 556	1.896	5.8
AMBPY-III	Rhombus	330	389,402, 558	1.799	2.6
Solution[b]	—	280	385	1.090	1.1

[a]average lifetime is calculated as described in ESI†, [b]in $CHCl_3$

is apparent from Table 1 that luminescence quantum yield in amorphous state is lower in comparison to the crystalline polymorphic state, indicating the possibility of CIEE phenomena. A 10-fold enhancement in fluorescence quantum yield of **AMBPY-II** is achieved in the polymorphic state relative to the amorphous solid and 5-fold increment with respect to the solution state. The differences in fluorescence quantum yield exhibited by **AMBPY** polymorphs could be corroborated to the differences in the π–π stacking interactions present in the three polymorphs. Seminal works by Jenekhe et al.[27] and Yamatao et al.[28] have shown that strong π–π stacking interactions can lead to extensive excimer formation in the solid state/thin films with a consequent reduction in the fluorescence quantum yield. We have evaluated the π–π stacking interaction between nearest neighbors (Fig. S12, ESI†) in each polymorph and the decreasing order of π–π interaction is as follows: **AMBPY-II** (3.752 Å) > **AMBPY-III** (3.598 Å) > **AMBPY-I** (3.477 Å). The same order is followed for the fluorescence quantum yield (Φ_f): **AMBPY-II** (Φ_f=5.8) > **AMBPY-III** (Φ_f=2.6) > **AMBPY-I** (Φ_f=2.4). As evident from the qualitative analysis, **AMBPY-I** possess strongest π–π stacking interaction between the nearest neighbors and hence have least Φ_f, whereas **AMBPY-II** with weakest π–π stacking interaction between nearest neighbors possesses highest Φ_f. Alteration in the contributions of the n-π* (forbidden) and π-π* (allowed) transitions (Fig. S10, ESI†) to the lowest absorption band could be induced by the differences in torsional angles thereby conformational fixation due to the crystal packing.[3a] The increase in Φ_f in polymorphs in comparison to the amorphous solid could also be due to the 4.18% increase in the radiative rate constant with respect to the amorphous state (Table S7, ESI†). The enhancement in the Φ_f of the polymorphs compared to the amorphous solid/solution state corresponds to the crystallization induced emission enhancement in the rotationally flexible polymorphs.

Conclusions

Three conformational polymorphs of 4-amino-2,2'-bipyridine crystallizing in distinct crystal systems is reported. Analyses of various interactions present in the polymorphs revealed that differences in the face-to-face interaction play decisive role in dictating the luminescence properties. Increase in the fluorescence quantum yield of crystalline polymorphs relative to the amorphous solid/solution state could be attributed to the CIEE. This strategy of regulating luminescent properties of molecular solids by virtue of packing at the molecular level could be exploited in the design and construction of various organic light emitting devices.

Acknowledgement

M. H. acknowledges Kerala State Council for Science, Technology and Environment (KSCSTE) for the support of this work, 007/KSYSA-RG/2014/KSCSTE. Authors thank Alex P. Andrews, IISER-TVM for X-ray crystal structure analyses. Ajith R. M. thanks CSIR; Ramarani Sethy and Vinayak Bhat thank INSPIRE Fellowship for the financial assistance. Authors thank Dr. Sunil Varghese, NIIST-Trivandrum for valuable suggestions.

Notes and references

Crystallographic data: for **AMBPY-I**: [C_{10} H_9 N_3], Mw = 171.20, hexagonal, space group $P6_5$, a = 18.260(2), b = 18.260(2), c = 5.0477(8) Å, α = 90°, β = 90°, γ = 120°, V= 1457.5(4) Å^3 , Z = 6, D_c = 1.170 g cm^{-3}, λ(Mo-Kα) = 0.7107 Å, T = 296(2) K, 7578 reflections collected, 1839 independent reflections (R_{int} = 0.0404), final R_1 [I > 2σ(I)] = 0.0530, final wR(F_2) = 0.1471 and CCDC number = 1427788. For **AMBPY-II**: [C_{10} H_9 N_3], Mw = 171.20, tetragonal, space group $I4_1/a$, a = 23.5825(14), b = 23.5825(14), c = 6.2166(5) Å, α = 90°, β = 90°, γ = 90°, V = 3457.3(4) Å^3 , Z = 16, D_c = 1.316 g cm^{-3}, λ(Mo-Kα) = 0.7107 Å, T = 296(2) K, 6425 reflections collected, 1524 independent reflections (R_{int} = 0.0186), final R1 [I > 2σ(I)] = 0.0418, final wR(F_2) = 0.1206 and CCDC number = 1427785. For **AMBPY-III**: [C_{10} H_9 N_3], Mw = 171.20, orthorhombic, space group Pccn, a = 15.2009(19), b = 9.7035(11), c = 12.0827(15) Å, α = 90°, β = 90°, γ = 90°, V = 1782.2(4) Å^3 , Z = 8, D_c = 1.276 g cm^{-3}, λ(Mo-Kα) = 0.7107 Å, T = 296(2) K, 7863 reflections collected, 1824 independent reflections (R_{int} = 0.0269), final R_1 [I > 2σ(I)] = 0.0511, final wR(F_2) = 0.1385 and CCDC number = 1427786.

1. S. Varughese, *J. Mater. Chem. C.*, 2014, **2**, 3499-3516.
2. D. Yan and D. G. Evans, *Materials Horizons*, 2014, **1**, 46-57.
3. (a) T. Mutai, H. Satou and K. Araki, *Nat. Mater.*, 2005, **4**, 685-687; (b) H. Y. Zhang, Z. L. Zhang, K. Q. Ye, J. Y. Zhang and Y. Wang, *Adv. Mater. (Weinheim, Ger.)*, 2006, **18**, 2369-2372.
4. X. He, A. C. Benniston, H. Saarenpaa, H. Lemmetyinen, N. V. Tkachenko and U. Baisch, *Chem. Sci.*, 2015, **6**, 3525-3532.
5. L. Yu, *Acc. Chem. Res.*, 2010, **43**, 1257-1266.
6. N. Zhao, M. Li, Y. Yan, J. W. Y. Lam, Y. L. Zhang, Y. S. Zhao, K. S. Wong and B. Z. Tang, *J. Mater. Chem. C.*, 2013, **1**, 4640-4646.
7. A. Qin and B. Z. Tang, *Aggregation-Induced Emission: Fundamentals and Applications*, John Wiley and Sons Ltd, 2013.
8. G. R. Desiraju, *Cryst. Growth Des.*, 2008, **8**, 3-5.
9. C. Liu, H. Luo, G. Shi, J. Yang, Z. Chi and Y. Ma, *J. Mater. Chem. C.*, 2015, **3**, 3752-3759.
10. (a) E. Elacqua, P. T. Jurgens, J. Baltrusaitis and L. R. MacGillivray, *CrystEngComm*, 2012, **14**, 7567-7571; (b) M. Kim, D. R. Whang, J. Gierschner and S. Y. Park, *J. Mater. Chem. C.*, 2015, **3**, 231-234.
11. (a) S. K. Rajagopal, A. M. Philip, K. Nagarajan and M. Hariharan, *Chem. Commun.*, 2014, **50**, 8644-8647; (b) R. T. Cheriya, K. Nagarajan and M. Hariharan, *J. Phys. Chem. C.*, 2013, **117**, 3240-3248; (c) K. Nagarajan, S. K. Rajagopal and M. Hariharan, *CrystEngComm*, 2014, **16**, 8946-8949.
12. (a) R. T. Cheriya, J. Joy, A. P. Alex, A. Shaji and M. Hariharan, *J. Phys. Chem. C.*, 2012, **116**, 12489-12498; (b) R. T. Cheriya, A. R. Mallia and M. Hariharan, *Energy Environ. Sci.*, 2014, **7**, 1661-1669.
13. Z. Zhou, G. H. Sarova, S. Zhang, Z. Ou, F. T. Tat, K. M. Kadish, L. Echegoyen, D. M. Guldi, D. I. Schuster and S. R. Wilson, *Chem. Eur. J.*, 2006, **12**, 4241-4248.
14. A. Bondi, *J. Phys. Chem.*, 1964, **68**, 441-451.
15. (a) W. Du, Q. Yin, J. Gong, Y. Bao, X. Zhang, X. Sun, S. Ding, C. Xie, M. Zhang and H. Hao, *Cryst. Growth Des.*, 2014, **14**, 4519-4525; (b) M. H. Abraham, *Chem. Soc. Rev.*, 1993, **22**, 73-83.
16. C. F. Macrae, P. R. Edgington, P. McCabe, E. Pidcock, G. P. Shields, R. Taylor, M. Towler and J. van de Streek, *J. Appl. Crystallogr.*, 2006, **39**, 453-457.
17. J. L. Atwood, L. J. Barbour, A. Jerga and B. L. Schottel, *Science*, 2002, **298**, 1000-1002.
18. S. Varughese, G. Cooke and S. M. Draper, *CrystEngComm*, 2009, **11**, 1505-1508.
19. M. A. Spackman and D. Jayatilaka, *CrystEngComm*, 2009, **11**, 19-32.
20. S. K. Wolff, D. J. Grinwood, J. J. McKinnon, M. J. Turner, D. Jayatilaka and M. A. Spackman, University of Western Australia, Perth, Australia, 2012.
21. L. Loots and L. J. Barbour, *CrystEngComm*, 2012, **14**, 300-304.
22. A. S. Batsanov, J. A. K. Howard, D. Albesa-Jové, J. C. Collings, Z. Liu, I. A. I. Mkhalid, M.-H. Thibault and T. B. Marder, *Cryst. Growth Des.*, 2012, **12**, 2794-2802.
23. J. J. McKinnon, D. Jayatilaka and M. A. Spackman, *Chem. Commun.*, 2007, 3814-3816.
24. S. Aitipamula and A. Nangia, *Chem. Commun.*, 2005, 3159-3161.
25. (a) K. Araki, T. Mutai, Y. Shigemitsu, M. Yamada, T. Nakajima, S. Kuroda and I. Shimao, *J. Chem. Soc.*, 1996, 613-617; (b) A. Weisstuch and A. C. Testa, *J. Phys. Chem.*, 1968, **72**, 1982-1987.
26. T. Smith and J. Guild, *Trans. Opt. Soc.*, 1931, **33**, 73.
27. (a) A. S. Shetty, E. B. Liu, R. J. Lachicotte and S. A. Jenekhe, *Chem. Mater.*, 1999, **11**, 2292-2295; (b) T. W. Kwon, M. M. Alam and S. A. Jenekhe, *Chem. Mater.*, 2004, **16**, 4657-4666.
28. J.-y. Hu, M. Era, M. R. J. Elsegood and T. Yamato, *Eur. J. Org. Chem.*, 2010, **2010**, 72-79.

Table of Graphical Contents